U. of Iowa 71:5

ON THE DISTRIBUTIONS OF PLASMAS AND ELECTRIC FIELDS OVER THE AURORAL ZONES AND POLAR CAPS*

by

L. A. Frank and D. A. Gurnett

Department of Physics and Astronomy

THE UNIVERSITY OF IOWA

Iowa City, Iowa

U. of Iowa 71-5

ON THE DISTRIBUTIONS OF PLASMAS AND ELECTRIC FIELDS OVER THE AURORAL ZONES AND POLAR CAPS*

by

L. A. Frank and D. A. Gurnett

February 1971

Department of Physics and Astronomy
The University of Iowa
Iowa City, Iowa 52240

*Research supported in part by the National Aeronautics and Space Administration under contracts NAS5-10625, NAS1-8141 and NAS1-2973 and grant NGL16-001-002 and by the Office of Naval Research under contract N000-14-68-A-0196-003.

Abstract

Simultaneous observations of DC electric fields and low-energy charged particles at low altitudes over the earth's auroral zones and polar caps were obtained with the satellite Injun 5. Several of the principal results for the evening and dawn local time sectors are summarized as follows.

1. The most prominent features of the convection electric fields are reversals located at high magnetic latitudes in the dawn and evening sectors.

2. The east-west convection velocity is usually anti-sunward at latitudes above the reversal boundary and sunward at latitudes below the reversal boundary.

3. The reversal is usually larger and more definitive in the dawn sector and relatively small and less definitive at local evening.

4. The convection electric field reversals in the dawn and evening sectors are coincident with the 'trapping boundary' for energetic electrons $E > 45$ keV. This trapping boundary is observationally identified with the high-latitude termination of measurable electron intensities as viewed with a detector with generous geometry factor. This trapping boundary is not synonymous with the high-latitude limit of durable trapping, i.e., an electron with these energies is not necessarily able to execute a complete longitudinal drift motion.

5. Over the polar caps the convection velocities are generally small, or below the instrumental threshold of $\sim$ 250 meters $(sec)^{-1}$, relative to the convection velocities in the vicinity of the reversals.

6. The polar cap region proper is $\sim$ 10° to 20° in latitudinal width, lies above the zone of anti-sunward convection, and is not necessarily centered at the magnetic pole but may be displayed toward local dawn or evening.

7. The polar cap region is characterized by an absence of measurable low-energy proton and electron intensities.

8. Inverted 'V' precipitation events, which are characterized with increasing average electron energies to a peak energy and a subsequent decrease in energy as the satellite passes through this intense precipitation event, are associated with the convection field reversals (and hence also the trapping boundaries) or with discontinuities in the convection field.

9. Field-aligned electron angular distributions occur at and above the trapping boundary and within the inverted 'V' precipitation events.

10. Proton and electron energy spectrums observed at latitudes above the trapping boundary are soft, and not dissimilar from proton and electron spectrums found in the polar cusp and high-latitude magnetotail (distant plasma sheet).

11. Diffuse precipitation zones of electron and proton intensities with spectrums similar to those observed in the near-earth plasma sheet are located at latitudes below the trapping boundary and within the region of sunward convection velocities. The ratios of intensities at pitch angles α = 0° to those measured at α = 90° (Northern hemisphere) are usually $\leq$ 1.

12. During a magnetic substorm the overall configuration of the convection velocities and plasma regions remained similar to those observed during quiescent periods except that convection velocities and particle intensities increased and the locations of these phenomena in magnetic latitude varied.

13. During the substorm the asymmetric injection of protons deep into the outer radiation zone to L = 3.8 during local evening was observed. The lowest L-value for measurable proton intensities as measured 15 minutes of elapsed time earlier in the local morning sector was L = 7.3.

These observations are interpreted in terms of a magnetospheric model as deduced from plasma observations in the distant magnetosphere and in terms of essential elements for any credible theory of auroral arcs, in particular those associated with inverted 'V' precipitation bands.

I. Introduction

Over the past several years it has become increasingly evident that simultaneous observations of the plasmas and electric fields above the auroral zones are a necessity for delineating the sources of auroral radiations. The techniques for measuring electric fields utilizing Ba^+ cloud releases [Haerendel and Lust, 1970; Wescott et al., 1970] and satellite instrumentation [Gurnett, 1970; Maynard and Heppner, 1970] have now been introduced successfully. A host of satellites employing a variety of low-energy particle detectors has already provided a survey of the plasmas above the auroral zones. A review of these measurements has been given by Hultqvist [1969]. Although measurements of both electric fields and plasmas at low altitudes over the polar caps, auroral zones and within the outer radiation zone are available, theoretical interpretations of such phenomena as auroral arcs are largely conjectural in nature. This situation arises in large part to the present inavailability of simultaneous observations of auroral electric fields and plasmas. Our purpose here is to summarize

the initial results of such a comparison of electric fields transverse to the local geomagnetic field vector and of the auroral corpuscular radiation as measured simultaneously with a low-altitude, polar-orbiting satellite.

II. Brief Description of Instrumentation

The earth-satellite Injun 5 was launched on 8 August 1968 into a near-polar orbit with inclination 81° and apogee and perigee altitudes 2528 and 677 km, respectively. The spacecraft was magnetically aligned with respect to the local magnetic field vector by means of two parallel bar magnets. A tape recorder with a bit rate of 800 bits $(\text{second})^{-1}$ provided world-wide surveys of plasma and electric fields. The second telemetry mode, 24,000 bits $(\text{second})^{-1}$, yielded high temporal resolution, real-time observations of auroral zone phenomena. Our current interest herein lies with survey measurements at moderate and high magnetic latitudes in the dawn-dusk meridional plane.

Low-energy charged particle detectors. Simultaneous observations of electron and proton intensities within the energy range $5 \leqslant E \leqslant 50{,}000$ eV were obtained with an array of electrostatic analyzers. A description of this instrumentation has been previously given [Frank et al., 1966]. For the present survey we shall utilize measurements obtained with two Low Energy Proton and Electron Differential Energy Analyzers (abbreviation, LEPEDEA), one with fields-of-view

directed anti-parallel to the local magnetic field vector (LEPEDEA 'A') and the other with fields-of-view directed perpendicular to this vector (LEPEDEA 'B'). Hence LEPEDEA 'A' measures the precipitated fluxes into the earth's atmosphere over the Northern hemisphere. Each of these analyzers provides observations of the directional, differential intensities of protons and electrons, separately and simultaneously. In the 'survey' mode of telemetry operation the instrument sensitivity, temporal resolution and energy range are sufficient to provide identification of the corresponding plasma regime in the distant magnetosphere, e.g., polar cap, plasma sheet, polar cusp, and proton ring current. Energetic electron intensities with $E > 45$ keV and associated phenomena such as the 'trapping boundary' were determined with a companion set of collimated, thin-windowed Geiger-Mueller tubes. For high-spatial and -temporal resolution studies of auroral phenomena the reader is referred to the survey given by Frank and Ackerson [1970]. However, all observations presented here were gathered in the 'survey' mode which permitted surveys over entire orbits via the satellite tape recorder and allowed us to establish the connections between the plasma phenomena and convection electric fields on a global scale at low altitudes.

DC electric field instrumentation. The DC electric field instrumentation has been described by Gurnett et al. [1969] and initial results have been presented by Gurnett [1970] and Cauffman and Gurnett [1971]. The electric field sensor consists of two conducting spheres mounted on booms with a center-to-center separation of 2.85 meters. The electric field component parallel to the axis through the spheres is determined by measuring the potential difference between the spheres with a high impedance voltmeter. The magnetic orientation of the satellite maintains the electric antenna axis perpendicular to the local geomagnetic field vector so that only the electric field component perpendicular to the geomagnetic field is sensed.

To determine the electric field due to magnetospheric plasma convection, the $\vec{V}_s \times \vec{B}$ electric field caused by the satellite motion through the ionosphere and small instrumental errors (due to asymmetrical sunlight shadowing of the spheres by the supporting booms) must be subtracted from the measured electric field. The detailed procedures used to determine this subtracted electric field are discussed by Cauffman and Gurnett [1971]. Since sunlight shadowing errors, which cannot be calculated directly, vary

slowly with the rotation of the satellite the accuracy with which the convection electric field can be determined depends on the time, or distance, scale of the phenomena. The rotation period of the spacecraft and thus also of the electric antenna axis around the local magnetic field vector is typically 20 minutes or longer. For distance scales of 1000 km or less, variations in the convection electric field can be determined with an accuracy ± 10 millivolts $(\text{meter})^{-1}$, or less, whereas over longer distance scales, 5000 km or greater, the accuracy of determination of the absolute convection electric field is normally limited to approximately ± 30 mv $(\text{meter})^{-1}$.

III. Observations

Two series of observations are presented here, one series for the Northern and Southern hemispheres during a period of relative magnetic quiescence and the second an example of plasma and electric field phenomena during a magnetic substorm.

Period of relative magnetic quiescence. Simultaneous observations of DC electric fields, energetic electron ($E > 45$ keV) intensities and lower energy electron ($1.6 \leq E \leq 2.5$ keV) intensities for a Northern polar pass on 7 February 1969 are shown in Figure 1. The observations for the following Southern polar pass are summarized in Figure 2. Magnetic local times MLT and invariant magnetic latitudes Λ as functions of Universal Time for these two polar passes are available in Figure 3. We have selected these passes on the basis of polar cap coverage at high latitudes, a dawn-dusk local time zone for the orbit and a period of relative magnetic quiescence ($K_p = 1^+$). The observations for this example are qualitatively similar to those for a series of such measurements under these conditions.

The DC electric field measurements, including the $\vec{V}_s \times \vec{B}$ field and uncorrected for any shadowing errors are

shown in the top panels of Figures 1 and 2. The systematic sinusoidal variation of the DC electric field with a period of approximately 22 minutes reflects the aforementioned rotation of the satellite in the $\vec{V}_s \times \vec{B}$ field. With the exception of the small perturbation labelled 'spacecraft body shadow' the deviations from the smooth sinusoidal $\vec{V}_s \times \vec{B}$ field are due to convection electric fields. The dashed lines in regions where significant convection electric fields are observed is the estimated $\vec{V}_s \times \vec{B}$ field and represents the 'zero reference' for determining the magnitude and sign of the convection electric field component detected.

The principal features of the DC electric field observations of Figures 1 and 2 are the abrupt reversals of these electric fields at 15:33 and 16:41 U.T. (magnetically conjugate points at local dawn) and the smaller, less definitive reversals at about 15:43 and 16:27 U.T. (local evening). These reversals in the sign of the convection electric field are a persistent feature of the DC electric field observations with Injun 5. As discussed by Cauffman and Gurnett [1971] this electric field reversal is associated with a reversal in the generally east-west direction of the

plasma convection, with the convection velocity directed sunward on the low latitude side of the reversal boundary and anti-sunward on the high latitude side. Over the polar cap region at latitudes above the reversal boundary, e.g., over the period 15:36 to 15:39 U.T. of Figure 1, the convection electric field is generally small compared to the convection electric fields observed near the reversal boundary.

In a following section we shall invoke simultaneous measurements of proton and electron intensities to identify the regions such as plasma sheet and polar cap in the distant magnetosphere which correspond to the convection zones discussed above. However, we have included observations of electron ($E > 45$ keV) intensities with pitch angles $\alpha = 90°$ in the middle panels of Figures 1 and 2 and of lower energy electron ($1.6 \leq E \leq 2.5$ keV) in the bottom panels. The energetic electron ($E > 45$ keV) intensity profiles provide a definitive determination of the 'trapping boundaries' at high latitudes. Observationally these boundaries are to be identified with the high-latitude termination of measurable electron intensities, e.g., at approximately 16:27 and 16:41 U. T. of Figure 2. The geometric factors of the Geiger-Mueller tubes used to obtain these observations are large,

~ 0.02 cm^2-sr, relative to those we have employed on previous satellites, and hence respond to relatively low intensities. We associate this 'trapping' boundary as coincident with the boundary between magnetic field lines closed within the magnetosphere (lower latitudes) and open field lines (higher latitudes) to the interplanetary medium. We will later reject the alternative interpretation invoking closed but unpopulated field lines over the polar cap with measurements of the low-energy particle distributions. These energetic electron intensities near the boundary are not necessarily durably trapped in the sense that an electron populating these higher latitude closed field lines will complete a longitudinal drift motion around the earth. With regards to the convection electric field this trapping boundary almost invariably is coincident with the reversal of the convection from sunward (lower latitude) to anti-sunward flow at higher latitudes. The observations of Figures 1 and 2 provide prominent examples of the striking correlation of these two phenomena.

Intensities of lower energy electrons, $1.6 \leq E \leq 2.5$ keV, at local pitch angle $\alpha = 90°$ are shown in the bottom panels of Figures 1 and 2. This energy range and pitch angle was

chosen as a coarse index to the regions of electron precipitation into the Northern and Southern auroral zones. Over the Northern hemisphere, these electron events were confined to latitudes within the outer radiation zone and were located equatorward of the trapping boundary. Inspection of the responses of the analyzers for other energy bandpasses provides identification of these precipitation events as the diffuse, structureless type with relatively hard electron spectrums observed at these local times as previously discussed by Frank and Ackerson [1970]. The observations over the Southern polar cap revealed a similar type of hard electron precipitation equatorward of the trapping boundary with the exception of the two maxima of intensities centered at 16:28 and 16:41 U.T. located near the trapping boundary and convection electric field reversals.

These two maxima of intensities are the signatures of a second type of precipitation event discussed by Frank and Ackerson [1970], the inverted 'V' electron precipitation event. These intense events are characterized by (1) rapidly decreasing differential intensities with increasing electron energy in the high-energy tail of the spectrum (soft spectrum), (2) widths typically $\sim$ 50 to 300 km and (3) average electron energy which rises from $\leqslant$ 100 eV

to a maximum energy ranging from $\sim$ several hundred eV to tens of kiloelectron volts and returns to $\leq$ 100 eV with the passage of the satellite through the precipitation band (evidenced by an inverted 'V' structure in energy-time spectrograms of these events). Again the reader is referred to the survey given by Frank and Ackerson [1970] for examples of these two types of precipitation events. Intense, soft electron events were also observed near the trapping boundaries for the Northern polar pass of Figure 1. However, the peak energies of the inverted 'V' substructure were low, $\sim$ several hundred eV, and there were no electron ($1.6 \leq E \leq 2.5$ keV) intensities exceeding the detector threshold intensity. We shall expand our discussion of the relationships of these precipitation events with respect to auroral and magnetospheric phenomena with the presentation of results obtained during a period of magnetic activity.

A further useful summary of the convection velocity components and the orbit for the series of measurements of Figures 1 and 2 is given in the magnetic local time-invariant latitude (MLT - Λ) polar diagram of Figure 3. Since only one component of the electric field is sensed, only the component of convection velocity perpendicular to the

axis of the electric antenna can be determined. The direction of the arrows in Figure 3 is in the direction of the convection velocity sensed, and the length of arrows is proportional to the magnitude of this velocity as computed from $V_c = E_c/B$, where E_c is the convection electric field obtained after subtracting the $\vec{V}_s \times \vec{B}$ field and shadowing errors from the measured electric field and B is the scalar value of the local geomagnetic field. It must be emphasized that the arrow represents only the component of the convection velocity detected; it does not represent the vector direction of the convection velocity since only one component is measured.

The electric field reversal at 15:33 U.T. in Figure 1 corresponds to the reversal in the east-west convection velocity shown in the dawn sector of the Northern hemisphere polar diagram of Figure 3. The characteristic reversal in the east-west convection in this region is particularly clear in this case because the electric antenna was aligned approximately north-south at this time and was measuring the east-west component of the convection velocity. On the high latitude side of the reversal, above the trapping boundary for energetic electrons (see Figure 1), the plasma convection is westward, away from the sun, and on the low-

latitude side of the reversal, equatorward of the trapping boundary, the convection velocity is eastward, toward the sun. In the Southern hemisphere the magnetically conjugate reversal at 16:41 U.T. is qualitatively the same although the antenna orientation is not as favorable for detecting east-west convection.

The smaller reversals on the dusk side of the polar region at 15:43 and 16:27 U.T. are also consistent with respect to the east-west component of the convection velocity in opposite hemispheres; with anti-sunward convection poleward of the trapping boundary and sunward convection equatorward of the trapping boundary.

The convection velocities shown in the polar diagram of Figure 3, although somewhat larger in magnitude than are usually observed, illustrate several features typical of the convection velocities observed in the dawn-dusk sectors with Injun 5: (1) the east-west convection velocity is usually anti-sunward at latitudes above the reversal boundary and sunward at latitudes below the reversal boundary, (2) the convection velocity over the polar region is usually small compared to the convection velocities observed in the reversal region, and (3) the reversal is usually larger in

magnitude and better defined in the dawn sector and smaller and less definitive in the dusk region.

Observations during a magnetic substorm. Measurements of the electric fields and particle intensities over the Northern hemisphere during a polar magnetic substorm on 13 March 1970 are summarized in Figure 4. The magnetograms acquired at College, Alaska, clearly show that a moderate magnetic substorm was in progress during these satellite observations while the magnetic observatory was located in the post-midnight local time sector. The corresponding magnetic disturbance index was $K_p = 3^-$. As we shall see the overall interrelationships of the various phenomena observed during these magnetic disturbances do not differ in character from the findings for periods of relative magnetic quiescence, the primary difference is evident in the magnitudes and position in latitude of the electric field and plasma phenomena. This series of observations was also selected for analysis, in addition to magnetic activity, because of the slow rotation rate of the satellite ($\sim$ 1 hour) and the favorable (approximately north-south) orientation of the electric field antenna for detecting the east-west component of the plasma convection.

The measurements of Figure 4 begin in the dawn local time sector and continue into the polar cap region and thence into local evening. A summary of the satellite position in MLT - Λ polar coordinates is found in Figure 5.

The DC electric field measurements obtained during this pass display a large electric field reversal at 14:43 U.T., in the dawn local time sector, and a smaller discontinuity at 14:53 U.T. in the local evening sector. Due to the slow rotation of the satellite and the complete absence of sunlight shadowing errors the convection electric field can be determined with exceptionally good accuracy during this pass, $\sim \pm$ 10 mv $(\text{meter})^{-1}$. Over the polar cap region, which was encountered from approximately 14:46 to 14:50 U.T., the convection electric field is essentially zero within the resolution of the measurements. The latitudinal width of the polar cap region is $\sim 12°$ and its midpoint is displaced toward local evening relative to the Northern magnetic pole (cf. Figure 5). The convection velocity components are also summarized in Figure 5. The east-west convection velocities observed during this pass are qualitatively similar to the convection patterns observed for the the magnetically quiescent period discussed earlier except that the reversal regions

are broader and the convection velocities are enhanced during the substorm.

The trapping boundary for energetic electron (E > 45 keV) intensities is coincident with the two major reversals at 14:43 and 14:53 U.T., as was found for periods of relative magnetic quiescence. This correlation is clearly discernible in Figure 4.

Low-energy proton ($290 \leq E \leq 455$ eV) intensities (second panel from top of Figure 4) are located poleward and equatorward of the trapping boundary in the dawn and dusk local time sectors. These proton intensities will be identified here via their energy spectrums as to their association with the high-latitude magnetotail (distant plasma sheet) and the near-earth plasma sheet [cf. Frank, 1970a; Frank and Ackerson, 1970].

Electron ($325 \leq E \leq 570$ eV) intensities provide a useful index as to the location of inverted 'V' precipitation events. These measurements are summarized in the bottom panel of Figure 4. As with observations during magnetic quiescence these events are located near or at the position of the trapping boundaries and electric field reversals at 14:43 and 14:53 U.T. The second, or poleward, precipitation event at 14:52 U.T. of the pair of evening inverted 'V' events

is also located near a feeble discontinuity of the convection electric field.

The observations over the polar cap proper for both quiescent and disturbed magnetic conditions presented here feature an absence of measurable low energy charged particle intensities and relatively weak convection electric fields (cf. Figures 1, 2 and 4). A similar absence of measurable particle intensities in the polar cap region of the distant polar magnetosphere has been recently reported by Frank [1970c].

Measurements of low-energy charged particle intensities within a few energy bandpasses such as those shown in Figures 1, 2 and 4 are adequate for a coarse determination of the location of major precipitation zones. However, the full capabilities of the analyzer array must be employed in order to identify positions for field-aligned currents, hard and soft precipitation zones, and plasma sheet protons. Such an analysis for the substorm observations of Figure 4 is presented in the block diagram of Figure 6. This diagram is a comprehensive roadmap for the various regions and plasma phenomena encountered during this Northern polar pass. A summary of the nature of the convection electric fields is

shown at the top of Figure 6. The charged particle phenomena are summarized in the bottom half of this diagram:

(1) Electron E > 45 keV 'trapping boundary', the high latitude termination of measurable intensities of electrons E > 45 keV,

(2) Proton spectrums, classified 'hard' or 'soft' on the presence or absence, respectively, of measurable intensities of protons E > 10 keV,

(3) Electron spectrums, classified 'hard' or 'soft' with the absence or presence, respectively, of large intensities of lower energy electrons, $50 \leqslant E \leqslant 400$ eV, (the soft spectrums are also characterized with a relatively rapid decrease of differential electron intensities with decreasing electron energy in the high energy tail of the spectrum, see also Frank and Ackerson [1970]),

(4) Electron angular distributions: $j(0°)/j(90°) \leqslant 1$, maximum intensities at pitch angle $\alpha = 90°$; or $j(0°)/j(90°) \geqslant 1$, field-aligned current directed out of the atmosphere assuming no significant upflux [see Ackerson and Frank, 1971],

(5) Electron inverted 'V' events, bands of electron precipitation characterized with average electron energies rising from $\leqslant$ 100 eV to a maximum energy typically ranging from several hundred eV to tens of kiloelectron volts and returning to $\leqslant$ 100eV with the passage of the satellite through this precipitation event (for examples of these intense events, see Frank and Ackerson [1970]), and

(6) Plasma region in distant magnetosphere: polar cap, identified by absence of measurable low-energy proton and electron intensities and of detectable convection electric fields; polar cusp and distant plasma sheet (high-latitude magnetotail), identified by presence of soft proton and electron spectrums with weak intensities, anti-sunward convection and local time sector [Frank, 1970a, c]; and near-earth plasma sheet, located

> equatorward of the trapping boundary and identified with measurable intensities of energetic electrons E > 45 keV and sunward convection, includes regions of hard proton and electron spectrums and is bounded at its poleward side by inverted 'V' events (the signature of this region at low altitudes includes the ring current at low magnetic latitudes and the plasma sheet proper at geocentric radial distances $\geq$ 20 R_E at the higher latitudes).

We shall summarize all of the observational results in the next section. However, although many features of this roadmap are obvious, it is of interest to cite the asymmetric injection of ring current protons into the local evening sector as an example. The satellite transit time from the low-latitude edge of the extraterrestrial ring current at 14:41:10 U.T. in the local morning sector to the corresponding position in the local evening sector at 14:55:40 U.T. was only $\sim$ 15 minutes. These two boundaries were located at Λ = 68.4° and 59.3° in the morning and evening sectors, respectively; the corresponding L-values were L = 7.3 and 3.8. A similar asymmetry was encountered during the following Southern pass, approximately one hour later. This asymmetric injection of proton intensities to L-values deep within the outer radiation zone at local evening during magnetic substorms is similar to that reported by Frank [1970b] utilizing measurements of proton intensities near the magnetic equatorial plane.

IV. Summary of Observations

Several typical examples of simultaneous plasma and DC electric field measurements at low altitudes over the earth's polar caps and auroral zones have been presented. These observations were obtained in the dawn and evening local time sectors. For the convenience of the reader we summarize here the principal observational results.

(1) The most prominent features of the convection electric fields are reversals located at high magnetic latitudes in the dawn and evening sectors (cf. Figure 2 at approximately 16:27 and 16:41 U.T.).

(2) The east-west convection velocity is usually anti-sunward at latitudes above the reversal boundary and sunward at latitudes below the reversal boundary (cf. Figure 3).

(3) The reversal is usually larger and more definitive in the dawn sector and relatively small and less definitive at local evening (cf. Figures 1 and 3).

(4) The convection electric field reversals in the dawn and evening sectors are coincident with the 'trapping boundary' for energetic electrons $E > 45$ keV. This trapping boundary is observationally identified with the high-latitude termination of measurable electron intensities as viewed with a detector with generous geometry factor. Examples of this trapping boundary are shown at 15:33 and 15:43 U.T. of Figure 1; this trapping boundary is not synonymous with

the high-latitude limit of durable trapping, i.e., an electron with these energies is not necessarily able to execute a complete longitudinal drift motion.

(5) Over the polar caps the convection velocities are generally small, or below the instrumental threshold of $\sim$ 250 meters $(sec)^{-1}$, relative to the convection velocities in the vicinity of the reversals (cf. Figures 3 and 5).

(6) The polar cap region proper is $\sim$ 10° to 20° in latitudinal width, lies above the zone of anti-sunward convection, and is not necessarily centered at the magnetic pole but may be displayed toward local dawn or evening (cf. Figures 3 and 5).

(7) The polar cap region is characterized by an absence of measurable low-energy proton and electron intensities (cf. Figures 1, 2, 4 and 6).

(8) Inverted 'V' precipitation events, which are characterized with increasing average electron energies to a peak energy and a subsequent decrease in energy as the satellite passes through this intense precipitation event as discussed by Frank and Ackerson [1970], are associated with the convection field reversals (and hence also the trapping boundaries) or with discontinuities of the convection fields (cf. Figures 4 and 6).

(9) Field-aligned electron angular distributions occur at and above the trapping boundary and within the inverted 'V' precipitation events (cf. Figure 6).

(10) Proton and electron energy spectrums observed at latitudes above the trapping boundary are soft, and not dissimilar from proton and electron spectrums found in the polar cusp and high-latitude magnetotail (distant plasma sheet) (cf. Figures 4 and 6).

(11) Diffuse precipitation zones of electron and proton intensities with spectrums similar to those observed in the near-earth plasma sheet are located at latitudes below the trapping boundary and within the region of sunward convection velocities (cf. Figures 1 and 6). The ratios of intensities at pitch angles $\alpha = 0°$ to those measured at $\alpha = 90°$ (Northern hemisphere) are usually ≤ 1.

(12) During a magnetic substorm the overall configuration of the convection velocities and plasma regions remained similar to those observed during quiescent periods except that convection velocities and particle intensities increased and the locations of these phenomena in magnetic latitude varied (cf. Figures 4, 5 and 6).

(13) During the substorm the asymmetric injection of protons deep into the outer radiation zone to L = 3.8 during local evening was observed. The lowest L-value for measurable proton intensities as measured 15 minutes of elapsed time earlier in the local morning sector was L = 7.3.

V. Interpretation and Discussion

Over the past few years several models of magnetospheric convection have been proposed to account for polar and magnetospheric substorms. A review of these models has been given by Axford [1969]. In our present interpretation of the observational features of convection patterns at low altitudes over the earth's auroral zones and polar caps, and of the plasmas in the distant magnetosphere and at low altitudes, we must reject such models as Dungey's [1961, 1968] which predict strong, uniform convection of magnetic field lines over the earth's polar caps. Although we shall retain herein Dungey's concept of the connection of geomagnetic field lines with those of the interplanetary medium as an important element of any magnetospheric model, several prominent observational features which are inconsistent with the topology of such models are (1) strong sunward convection below the trapping boundary for energetic electrons and strong anti-sunward convection in a zone lying above this boundary and relatively small or no convection over the polar cap at low altitudes, (2) the overall absence of low-energy magnetosheath protons and electrons over the earth's polar caps, and (3) the character of the direct

entry of magnetosheath plasma into the dayside magnetosphere and the barren nature of the distant polar cap region with regards to its population of low-energy proton and electron intensities [Frank, 1970c].

A magnetospheric model based upon observations of low-energy charged particle intensities in the distant polar magnetosphere and near the magnetic equatorial plane has been recently proposed by Frank [1970c, d]. The convection electric fields and overall character of the charged particle distributions encountered at low altitudes over the polar caps and auroral zones as reported here are in qualitative agreement with this model. A diagram of the pertinent elements of this magnetospheric model is shown in Figure 7. Magnetic merging along the sunlit magnetopause allows the direct entry of magnetosheath plasma into the magnetosphere via the polar cusps. Polar cusp field lines, B and b, are connected to interplanetary field lines in the magnetosheath. Field lines, B and b, within the polar cusps are convected in the anti-solar direction into the distant plasma sheet (magnetic field lines B' and b'). The distant plasma sheet is the topological extension of the polar cusp into the magnetotail. Merging at the neutral sheet in the magnetotail provides the closed

field lines, A, within the near-earth plasma sheet. These field lines are convected sunward toward the sunlit magnetopause. Not all field lines of the type, B' and b', in the distant plasma sheet merge in the magnetotail. The alternative history of these field lines is to be vacated of magnetosheath plasma as the plasma flows downstream from the earth, subsequently to become polar cap field lines. The convection patterns expected over the polar caps have been discussed by Frank [1970d]. The model predicts low convection velocities relative to those at the polar cusp intersection with the ionosphere and directed sunward (cf. Figures 3 and 5). Magnetic field lines, B' and b', of the distant plasma sheet lie at latitudes above those of the near-earth plasma sheet, A, (see 'interior field configuration' of Figure 6); these field lines at geocentric radial distances $\sim$ 10 to 30 R_E have also been called the 'high-latitude' magnetotail. The energy spectrums of proton and electron intensities in the polar cusp, distant plasma sheet and high-latitude magnetotail are soft relative to those of the near-earth plasma sheet [cf. Frank 1970a, 1970c; Frank and Ackerson, 1970].

The strong dawn-dusk asymmetry in the intensities of the convection electric fields as reported here appears difficult to account for with any closed-field-line model of the magnetosphere. Since magnetic merging is sensitive to the direction of the interplanetary magnetic field, it is not unreasonable to expect a frequent dawn-dusk asymmetry of convection velocities for open-field-line models in response to the average direction of the interplanetary field, i.e., at the magnetopause at late morning.

For orientation of the reader it is of interest to consider the implications of this magnetospheric model concerning the phenomena encountered with a low-altitude, polar-orbiting satellite. Let us return to Figure 6 and consider the simplest example, a satellite pass at the local noon meridian. If the satellite is moving equatorward from the polar cap region, it will first encounter the polar cusp (B and b) and enter the inner magnetosphere (A'). For a pass at local midnight, the satellite will pass from the polar cap region, into the high-latitude magnetotail (B' and b') and thence into the near-earth plasma sheet (A). Similar passes at local morning and evening are topologically somewhat more complex but are directly pertinent to the observations reported here. A satellite pass

from the polar cap region equatorward in these local time zones will pass in sequence through the polar cap region, the polar cusp (B and b) and/or the distant plasma sheet B' and b', and finally into the near-earth plasma sheet (A).

We have examined a series of low-altitude passes for low-energy proton intensities in the polar cusp region and its topological extension into the magnetotail, the distant plasma sheet, and find that the maximum intensities of these magnetosheath protons occur over the sunlit ionosphere. Corresponding intensities in the distant plasma sheet are considerably less. The detailed study of these distributions will presently be published. These spatial distributions of magnetosheath proton intensities are qualitatively in agreement with those deduced by Eather and Mende [1970] from photometric surveys. The various plasma regimes in the distant magnetosphere and the magnetic field line types for the substorm observations of Figures 4 and 5 are summarized in Figure 6.

As noted previously by Frank and Ackerson [1970] maximum energy fluxes precipitated into the earth's atmosphere frequently occur in the center of an inverted 'V' precipitation event. We associate these intense bands of electron precipitation with auroral arcs and our following comments

are directed toward pursuing further the mechanisms and conditions responsible for these precipitation events.

These inverted 'V' precipitation events are located in the vicinity of reversals or discontinuities in the convection electric fields. Returning to the electric field reversal at local dawn as shown in Figures 4 and 5, we note that the electric antenna axis was aligned approximately north-south, parallel to the satellite velocity vector, so that the electrostatic potential Φ in the reversal region can be determined from the electric field E,

$$\Phi = -\int E \, ds$$

where ds is an element of length along the satellite trajectory. This method of determining the electrostatic potential is valid only if the electric field variations are primarily spatial, such as is expected to be the case for electric field reversals of the type shown in Figure 4.

The north-south component of the electric field reversal in the local dawn sector during a substorm as shown in Figure 4 is displayed in the bottom panel of Figure 8. The $\vec{V}_s \times \vec{B}$ field due to the satellite motion along its trajectory has been subtracted. The electrostatic potential obtained by integrating the convection electric field along the satellite trajectory is shown in the middle panel of Figure 8. We have arbitrarily chosen the zero

of the electrostatic potential curve as located at 14:40 U.T. when the spacecraft was at the lowest latitude for detection of a convection electric field. At the time t_r for the encounter of the midpoint of the reversal at 14:43:20 U.T. the electrostatic potential reaches a maximum of +56 kilovolts.

Observations of the low-energy proton and electron intensities and their relationship to such phenomena as the trapping boundary and the plasma regimes of the distant magnetosphere are summarized in the top panel of Figure 8 and in Figure 6. The high-latitude boundary of the near-earth plasma sheet is chosen to coincide with the position of the trapping boundary. However, the character and directions of the convection electric fields and the penetration of low-energy plasma equatorward of the trapping boundary in a narrow zone which is $\sim 1°$ in latitudinal width and centered at 14:43:20 U.T. is interpreted here as implying that the boundary between open and closed magnetospheric field lines is not sharply defined (cf. Figures 4 and 6). In other words, it appears that this narrow zone comprises both open and closed field lines and is topologically mapped into a relatively broad region of reconnection of magnetic field lines, $\geq 10\ R_E$, along the neutral sheet in the magnetotail.

The most prominent feature of the auroral electron precipitation event is the inverted 'V' event shown in Figure 8. As stressed by Frank and Ackerson [1970] these bands of precipitation are encountered frequently and often are the principal contributors to the energy influx into the earth's upper atmosphere. These events are characterized with low average electron energies as the satellite initially enters the precipitation band, with a subsequent increase of average electron energy to a maximum and finally followed by a decrease to lower energies as the satellite passes through this band. This event as detected in the satellite survey mode of operation is depicted in the E-t diagram (spectrogram) of Figure 8. The time t_p for peak electron energy coincided with the encounter time t_r for the peak of the electrostatic potential profile within the observational resolution of ± 12 seconds. We are currently correlating high-time resolution observations to verify these relative encounter times within a resolution of ± 1 second. This correlation of electrostatic potential with the inverted 'V' electron precipitation event is strongly suggestive of an electrostatic acceleration mechanism which invokes electric fields parallel to the magnetic field in a narrow latitudinal zone located near or at the reversal of the convection electric fields.

The inverted 'V' electron events are characterized with angular distributions of intensities peaked along the magnetic field for electron energies $\leq$ several keV and are a current directed out of the ionosphere. If we apply the results of the previous discussion which suggests that these events are the signature of the electrostatic potential, we would expect that the direction of these parallel electric fields could reverse at either side of this event since the electrostatic potential is decreasing; this reversal of parallel electric fields would provide a return current down into the ionosphere (for example, low energy electrons out of the ionosphere). We have been searching for the signature of such a return current with measurements of low energy electrons ($5 \leq E \leq 100$ eV) over the Southern pole when the instrumentation is capable of viewing charged particle upfluxes from the auroral zones [Gurnett and Frank, 1971]. Our preliminary results from a study of several passes show that such intense field-aligned electron intensities do exist and are located in the vicinity of the inverted 'V' precipitation events.

In summary we consider the following observational and interpretive results as essential to any credible theory of auroral arcs, in particular those associated with inverted 'V' precipitation events.

(1) Auroral arcs are associated with reversals or discontinuities in the directions of convection electric fields as observed at low altitudes.

(2) These reversals are often identified with boundaries of plasma regimes within the distant magnetosphere, such as the polar cusp, distant plasma sheet and near-earth plasma sheet. Frequently these arcs occur at the boundary between the distant and near-earth plasma sheets, plasma regimes which are characterized by solar and anti-solar convection, respectively. Magnetic merging and the subsequent collapse of closed magnetic field lines in the magnetotail are presumably the agents responsible for the sunward convection, but appear not necessary for producing an inverted 'V' event.

(3) Inverted 'V' electron precipitation events occur at or above the trapping boundary on open field lines. Hence there is essentially no 'lifetimes' for these events in terms of total number of electrons populating a field line (i.e., 'lifetime' for emptying a tube of force of its electrons). However, an upper limit on the electron densities is provided by the corresponding electron densities in the distant plasma sheet and down-stream magnetosheath. To our knowledge this upper limit, $\sim$ 10 to 100 $(cm)^{-3}$ has not been exceeded [cf. Frank and Ackerson, 1970].

(4) Multiple inverted 'V' events, or multiple arcs, are associated with multiple convection field reversals or discontinuities which reflect differential motions of plasmas in the polar cusps and distant plasma sheet. These convection field reversals are not necessarily topologically connected to a region of magnetic merging.

(5) Auroral arcs of this type are associated with high-β plasmas which are convecting within the distant magnetosphere.

(6) The signature of the inverted 'V' event in energy-time spectrograms of electron intensities and its frequent appearance near or at the peak of the convection electrostatic potential strongly imply that the acceleration mechanism proceeds via parallel electric fields.

(7) The angular distributions of electron intensities at energies $\leqslant$ several keV are peaked along the magnetic field direction. This observation provides support for a mechanism for accelerating these electrons in the vicinity of the earth (i.e., within geocentric radial distances $\leqslant 4$ or 5 R_E). Similar conclusions based upon various types of observations, such as those of time-delays of arrival and of angular distributions at low altitudes, have been forwarded previously [Hoffman and Evans, 1968; Frank and Ackerson, 1970].

Acknowledgments

This research was supported in part by the National Aeronautics and Space Administration under contracts NAS5-10625, NAS1-8141 and NAS1-2973 and grant NGL16-001-002 and by the Office of Naval Research under contract N000-14-68-A-0196-003.

References

Ackerson, K. L., and L. A. Frank, Correlated ground-based measurements of a visible auroral arc and low-energy electron precipitation, J. Geophys. Res. (to be submitted), 1971.

Axford, W. I., Magnetospheric convection, Rev. of Geophysics, 7, 379-419, 1969.

Cauffman, D. P., and D. A. Gurnett, Double probe measurements of DC electric fields with the Injun 5 satellite, J. Geophys. Res. (submitted for publication), 1971.

Dungey, J. W., Interplanetary magnetic field and the auroral zones, Phys. Res. Letters, 6, 47-48, 1961.

Dungey, J. W., The reconnection model of the magnetosphere, in Earth's Particles and Fields, ed. by B. M. McCormac, pp. 385-392, Reinhold Publishing Co., New York, 1968.

Eather, R. H., and S. B. Mende, Auroral precipitation patterns, Boston College Res. Rep., 1970.

Frank, L. A., Further comments concerning low energy charged particle distributions within the earth's magnetosphere and its environs, in Particles and Fields in the Magnetosphere, ed. by B. M. McCormac, pp. 320-331, Reinhold Publishing Co., New York, 1970a.

Frank, L. A., Direct detection of asymmetric increases of extraterrestrial 'Ring Current' proton intensities in the outer radiation zone, J. Geophys. Res., 75, 1263-1268, 1970b.

Frank, L. A., Plasma in the earth's polar magnetosphere, J. Geophys. Res. (submitted for publication), 1970c.

Frank, L. A., Comments on a proposed magnetospheric model, J. Geophys. Res. (accepted for publication), 1970d.

Frank, L. A. and K. L. Ackerson, Observations of charged particle precipitation into the auroral zone, J. Geophys. Res. (submitted for publication), 1970.

Frank, L. A., W. W. Stanley, R. H. Gabel, D. C. Enemark, R. F. Randall and N. K. Henderson, Technical description of LEPEDEA instrumentation (Injun 5), U. of Iowa Res. Rep. 66-31, 1966.

Gurnett, D. A., Satellite measurements of DC electric fields in the ionosphere, in Particles and Fields in the Magnetosphere, ed. by B. M. McCormac, pp. 239-246, D. Reidel Publishing Company, Dordrecht, Holland, 1970.

Gurnett, D. A., and L. A. Frank, VLF radio noise and plasma observations in the auroral zone, J. Geophys. Res. (to be submitted), 1971.

Gurnett, D. A., G. W. Pfeiffer, R. R. Anderson, S. R. Mosier, and D. P. Cauffman, Initial observations of VLF electric and magnetic fields with the Injun 5 satellite, J. Geophys. Res., 74, 4631-4648, 1969.

Haerendel, G., and R. Lust, Electric fields in the ionosphere and magnetosphere, in Particles and Fields in the Magnetosphere, ed. by B. M. McCormac, pp. 213-228, D. Reidel Publishing Company, Dordrecht, Holland, 1970.

Hoffman, R. A., and D. S. Evans, Field-aligned electron bursts at high latitudes observed by OGO 4, J. Geophys. Res., 73, 6201-6214, 1968.

Hultqvist, B., Auroras and polar substorms: observations and theory, Rev. of Geophys., 7, 129-177, 1969.

Maynard, N. C., and J. P. Heppner, Variations in electric fields from polar orbiting satellites, in Particles and Fields in the Magnetosphere, ed. by B. M. McCormac, pp. 247-253, D. Reidel Publishing Company, Dordrecht, Holland, 1970.

Wescott, E. M., J. D. Stolarik and J. P. Heppner, Auroral and polar cap electric fields from barium releases, in Particles and Fields in the Magnetosphere, ed. by B. M. McCormac, pp. 229-238, D. Reidel Publishing Company, Dordrecht, Holland, 1970.

Figure Captions

Figure 1. Simultaneous observations of DC electric fields due to magnetospheric plasma convection and of electron intensities over the Northern auroral zone and polar cap on 7 February 1969. The $\vec{V}_s \times \vec{B}$ field is the electric field attributed to the satellite motion through the earth's magnetic field. This period of observations for the dawn and evening local time sectors was characterized by relative magnetic quiescence ($K_p = 1^+$).

Figure 2. Continuation of Figure 1 for the following Southern polar pass approximately one hour later.

Figure 3. Polar diagram for the convection velocity component of the electric field observations displayed in Figures 1 and 2. The coordinates are magnetic local time (MLT) and invariant latitude (Λ).

Figure 4. Simultaneous observations of proton and electron intensities at local pitch angle $\alpha = 90°$ and of DC electric fields for a Northern polar pass on 13 March 1970. With increasing Universal Time the satellite passed over the auroral zone at local dawn, the polar cap region, and the auroral zone at local evening. A moderate substorm was in progress as evidenced in the magnetograms obtained at College, Alaska, which was in the post-midnight sector. The magnetic index $K_p = 3^-$.

Figure 5. A MLT - Λ polar diagram for the convection velocity components derived from the DC electric field observations of Figure 4.

Figure 6. A 'roadmap' for the various plasma regions and convection zones as functions of Universal Time for observations during the Northern polar pass of Figure 4.

Figure 7. Schematic diagram for the relationship of plasma and convection regions at low altitudes with the topology and plasma regimes of the distant magnetosphere. (See text.)

Figure 8. Summary of several prominent features of convection electric fields and low-energy charged particle intensities as the satellite Injun 5 passed over an auroral arc centered at approximately 14:43:20 U.T. on 13 March 1970. (See also Figures 4, 5, and 6.)

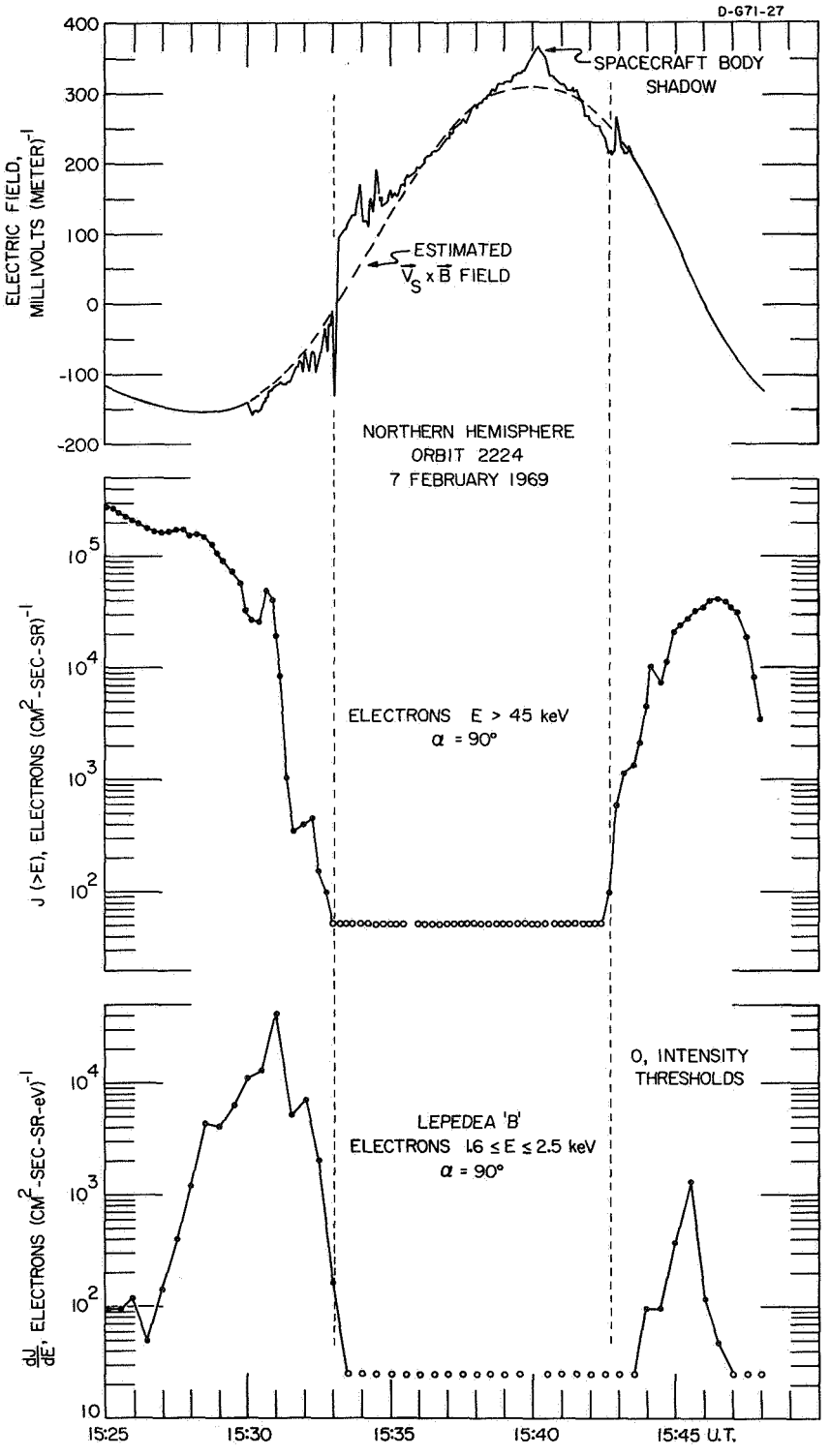
D-G71-27
ELECTRIC FIELD, MILLIVOLTS (METER)$^{-1}$
400
300
200
100
0
-100
-200
SPACECRAFT BODY SHADOW
ESTIMATED $\vec{V}_S \times \vec{B}$ FIELD
NORTHERN HEMISPHERE
ORBIT 2224
7 FEBRUARY 1969
J (>E), ELECTRONS (CM^2-SEC-SR)$^{-1}$
10^5
10^4
10^3
10^2
ELECTRONS E > 45 keV
α = 90°
$\frac{dJ}{dE}$, ELECTRONS (CM^2-SEC-SR-eV)$^{-1}$
10^4
10^3
10^2
10
LEPEDEA 'B'
ELECTRONS 1.6 ≤ E ≤ 2.5 keV
α = 90°
O, INTENSITY THRESHOLDS
15:25
15:30
15:35
15:40
15:45 U.T.

Figure 1.

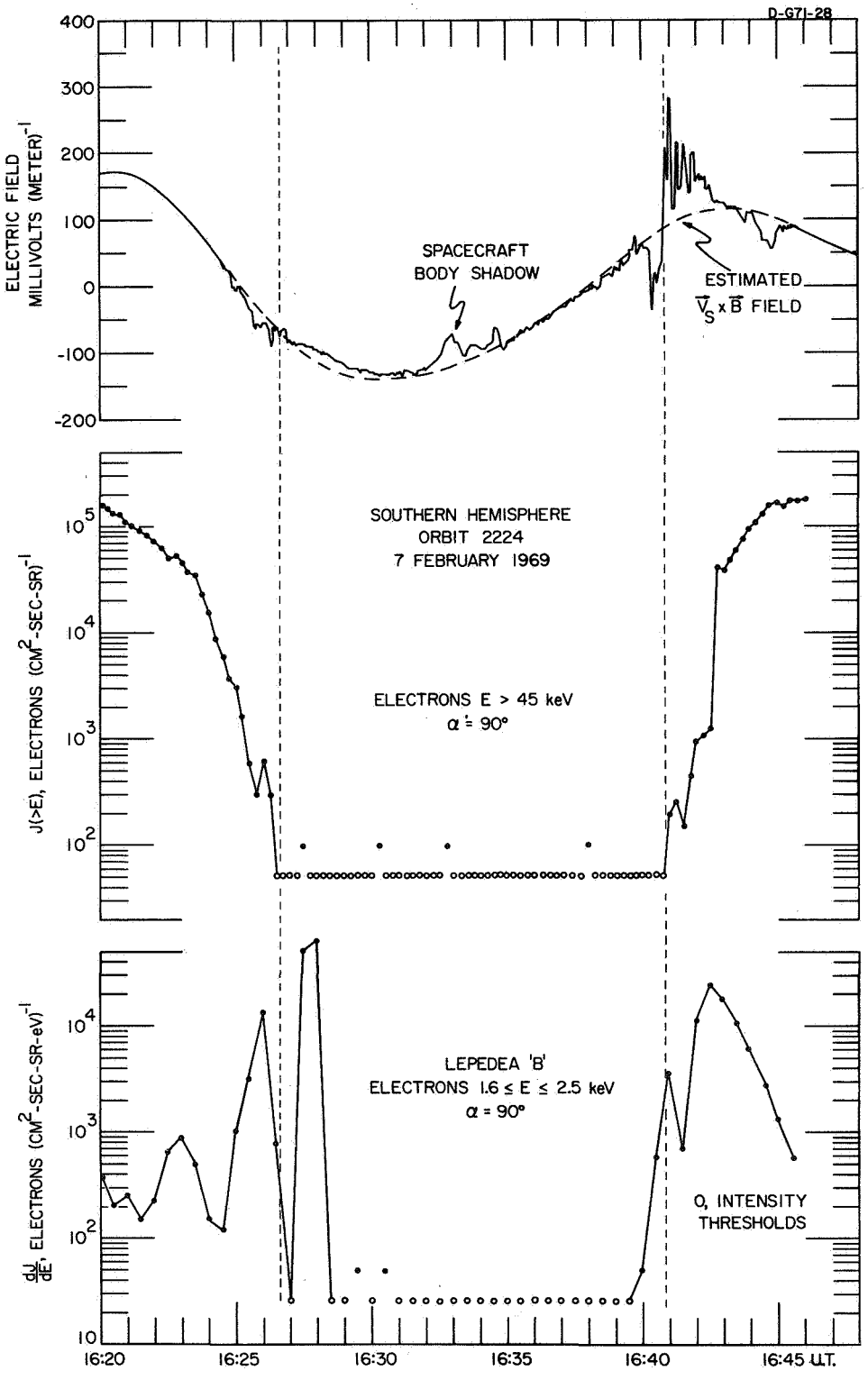
D-G71-28
ELECTRIC FIELD
MILLIVOLTS (METER)$^{-1}$
400
300
200
100
0
-100
-200
SPACECRAFT
BODY SHADOW
ESTIMATED
$\vec{V}_S \times \vec{B}$ FIELD
SOUTHERN HEMISPHERE
ORBIT 2224
7 FEBRUARY 1969
J(>E), ELECTRONS (CM^2-SEC-SR)$^{-1}$
10^5
10^4
10^3
10^2
ELECTRONS E > 45 keV
$\alpha \doteq 90°$
$\frac{dJ}{dE}$, ELECTRONS (CM^2-SEC-SR-eV)$^{-1}$
10^4
10^3
10^2
10
LEPEDEA 'B'
ELECTRONS 1.6 ≤ E ≤ 2.5 keV
$\alpha = 90°$
O, INTENSITY
THRESHOLDS
16:20
16:25
16:30
16:35
16:40
16:45 U.T.

Figure 2.

C-G71-49

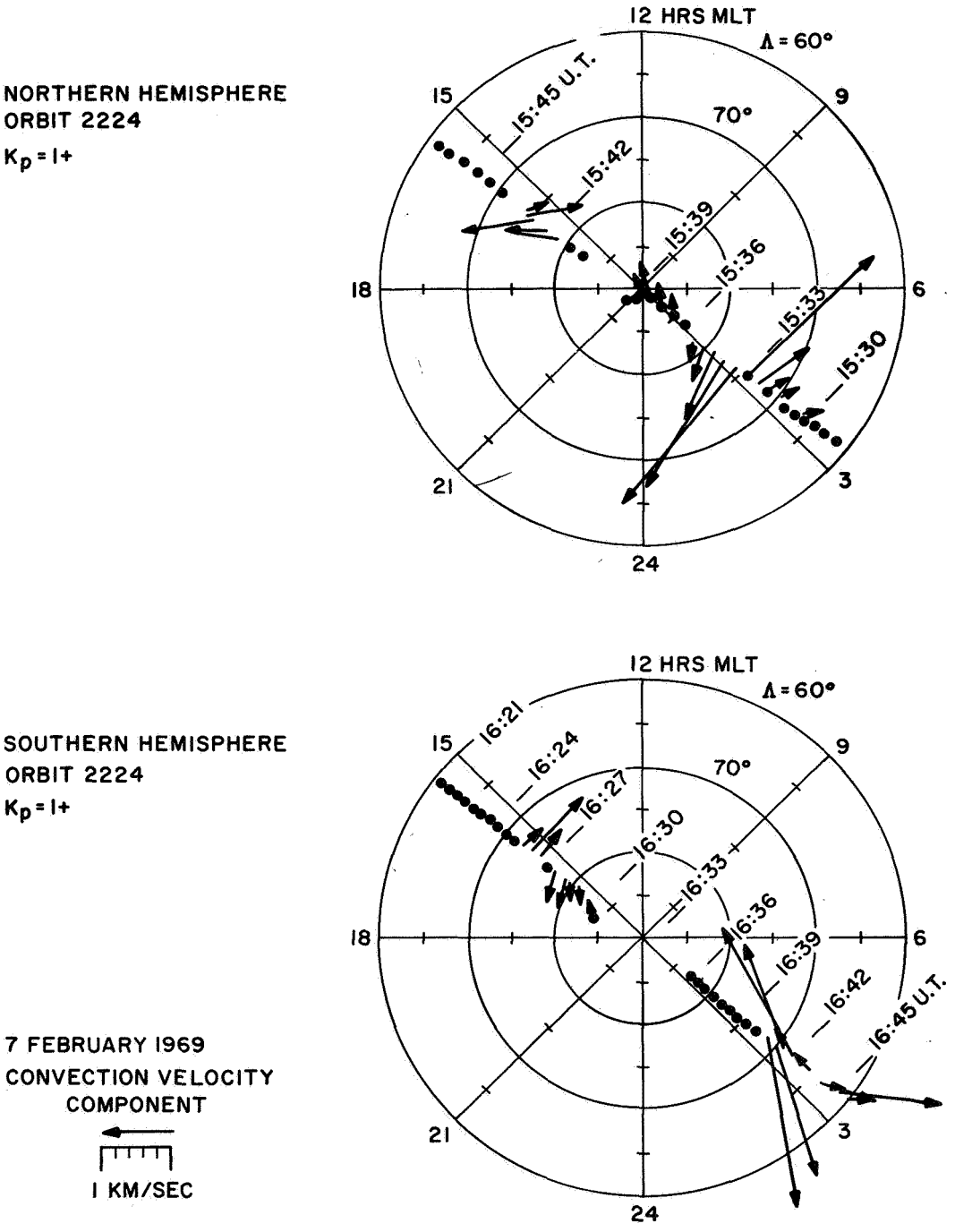

Figure 3.

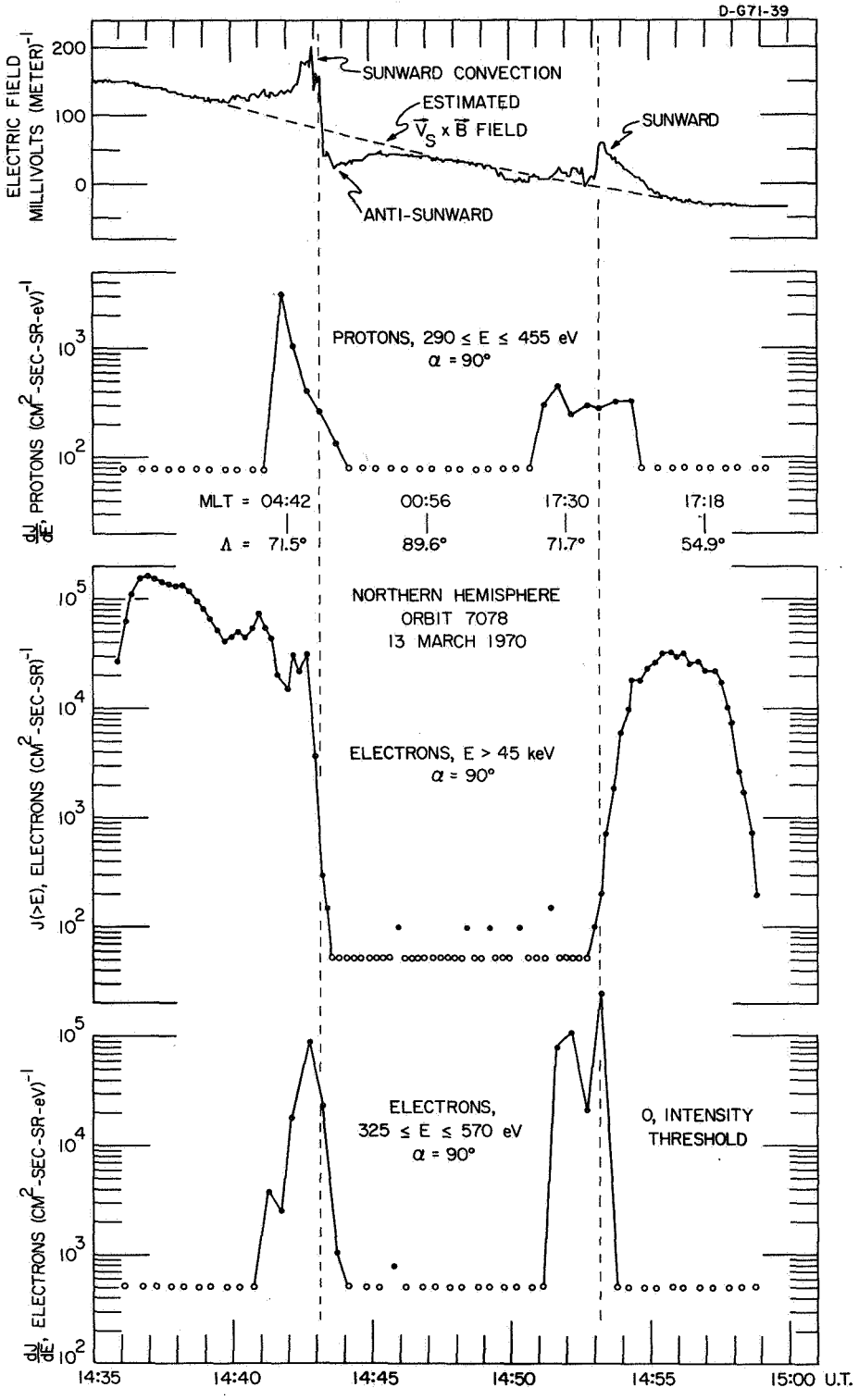
D-G71-39
ELECTRIC FIELD MILLIVOLTS (METER)$^{-1}$
200
100
0
SUNWARD CONVECTION
ESTIMATED
$\vec{V}_S \times \vec{B}$ FIELD
SUNWARD
ANTI-SUNWARD
$\frac{dJ}{dE}$, PROTONS (CM^2-SEC-SR-eV)$^{-1}$
10^3
10^2
PROTONS, 290 ≤ E ≤ 455 eV
α = 90°
MLT = 04:42
Λ = 71.5°
00:56
89.6°
17:30
71.7°
17:18
54.9°
J(>E), ELECTRONS (CM^2-SEC-SR)$^{-1}$
10^5
10^4
10^3
10^2
NORTHERN HEMISPHERE
ORBIT 7078
13 MARCH 1970
ELECTRONS, E > 45 keV
α = 90°
$\frac{dJ}{dE}$, ELECTRONS (CM^2-SEC-SR-eV)$^{-1}$
10^5
10^4
10^3
10^2
ELECTRONS,
325 ≤ E ≤ 570 eV
α = 90°
O, INTENSITY
THRESHOLD
14:35
14:40
14:45
14:50
14:55
15:00 U.T.

Figure 4.

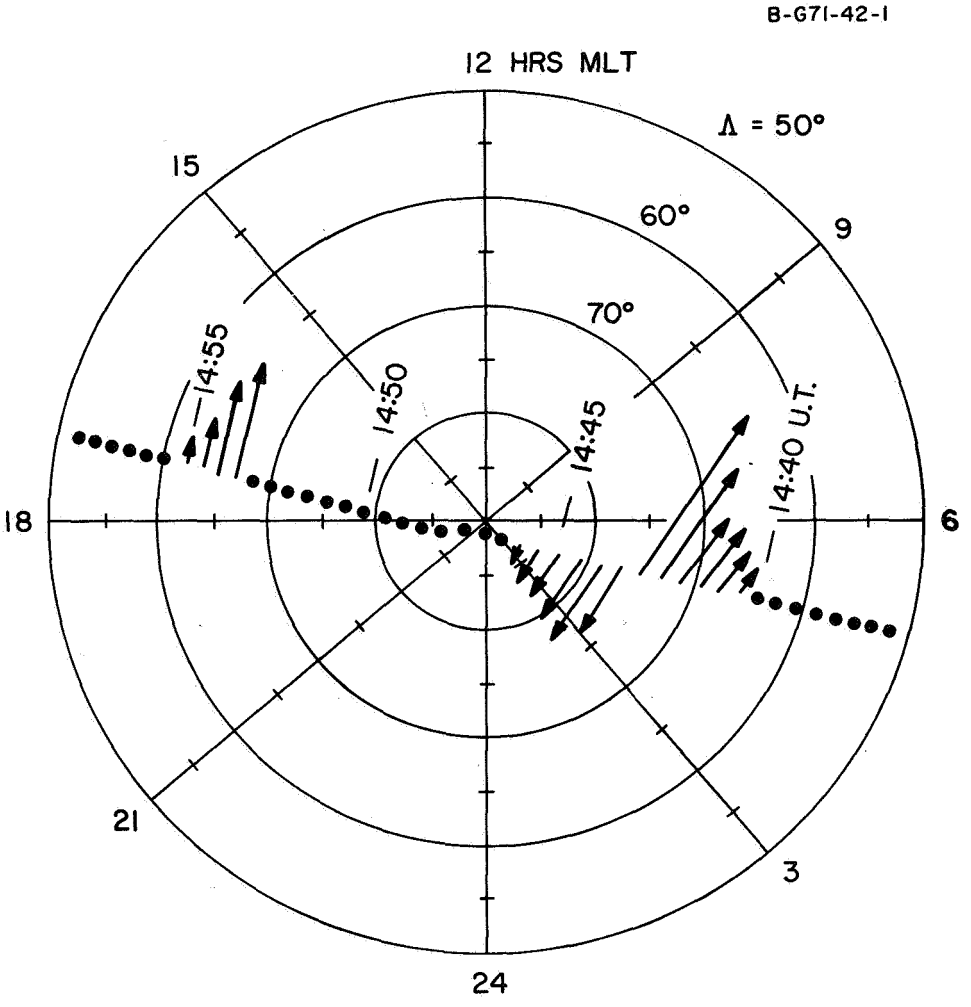
B-G71-42-1
12 HRS MLT
Λ = 50°
60°
70°
15
9
18
6
21
3
24
14:55
14:50
14:45
14:40 U.T.
13 MARCH 1970
CONVECTION VELOCITY COMPONENT
1 KM/SEC

Figure 5.

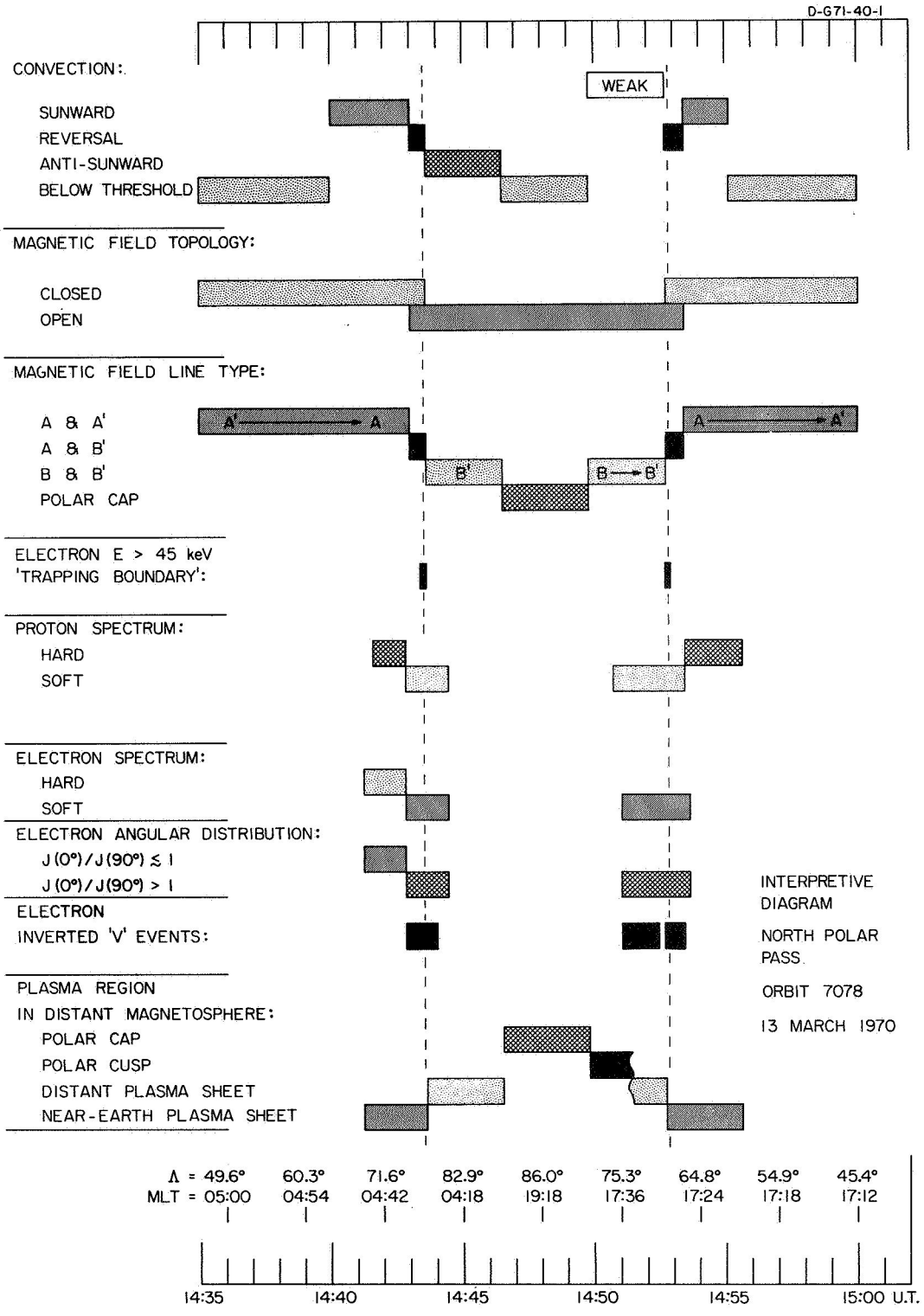
D-G71-40-1
CONVECTION:
WEAK
SUNWARD
REVERSAL
ANTI-SUNWARD
BELOW THRESHOLD
MAGNETIC FIELD TOPOLOGY:
CLOSED
OPEN
MAGNETIC FIELD LINE TYPE:
A & A'
A & B'
B & B'
POLAR CAP
A'
A
B'
B
B'
A
A'
ELECTRON E > 45 keV
'TRAPPING BOUNDARY':
PROTON SPECTRUM:
HARD
SOFT
ELECTRON SPECTRUM:
HARD
SOFT
ELECTRON ANGULAR DISTRIBUTION:
J(0°)/J(90°) ≲ 1
J(0°)/J(90°) > 1
ELECTRON
INVERTED 'V' EVENTS:
PLASMA REGION
IN DISTANT MAGNETOSPHERE:
POLAR CAP
POLAR CUSP
DISTANT PLASMA SHEET
NEAR-EARTH PLASMA SHEET
INTERPRETIVE
DIAGRAM
NORTH POLAR
PASS
ORBIT 7078
13 MARCH 1970
Λ = 49.6° 60.3° 71.6° 82.9° 86.0° 75.3° 64.8° 54.9° 45.4°
MLT = 05:00 04:54 04:42 04:18 19:18 17:36 17:24 17:18 17:12
14:35 14:40 14:45 14:50 14:55 15:00 U.T.

Figure 6

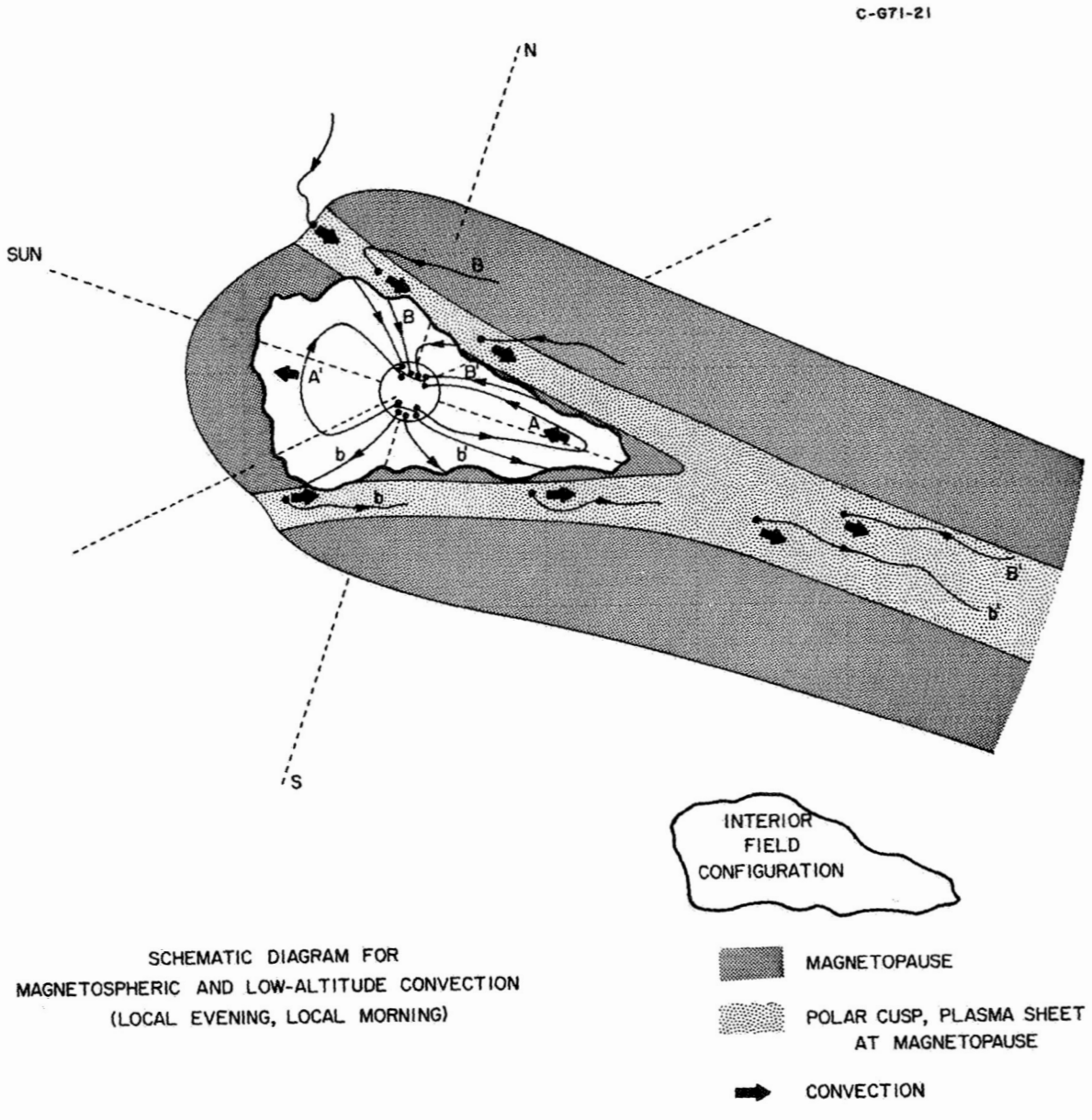

SCHEMATIC DIAGRAM FOR
MAGNETOSPHERIC AND LOW-ALTITUDE CONVECTION
(LOCAL EVENING, LOCAL MORNING)

Figure 7

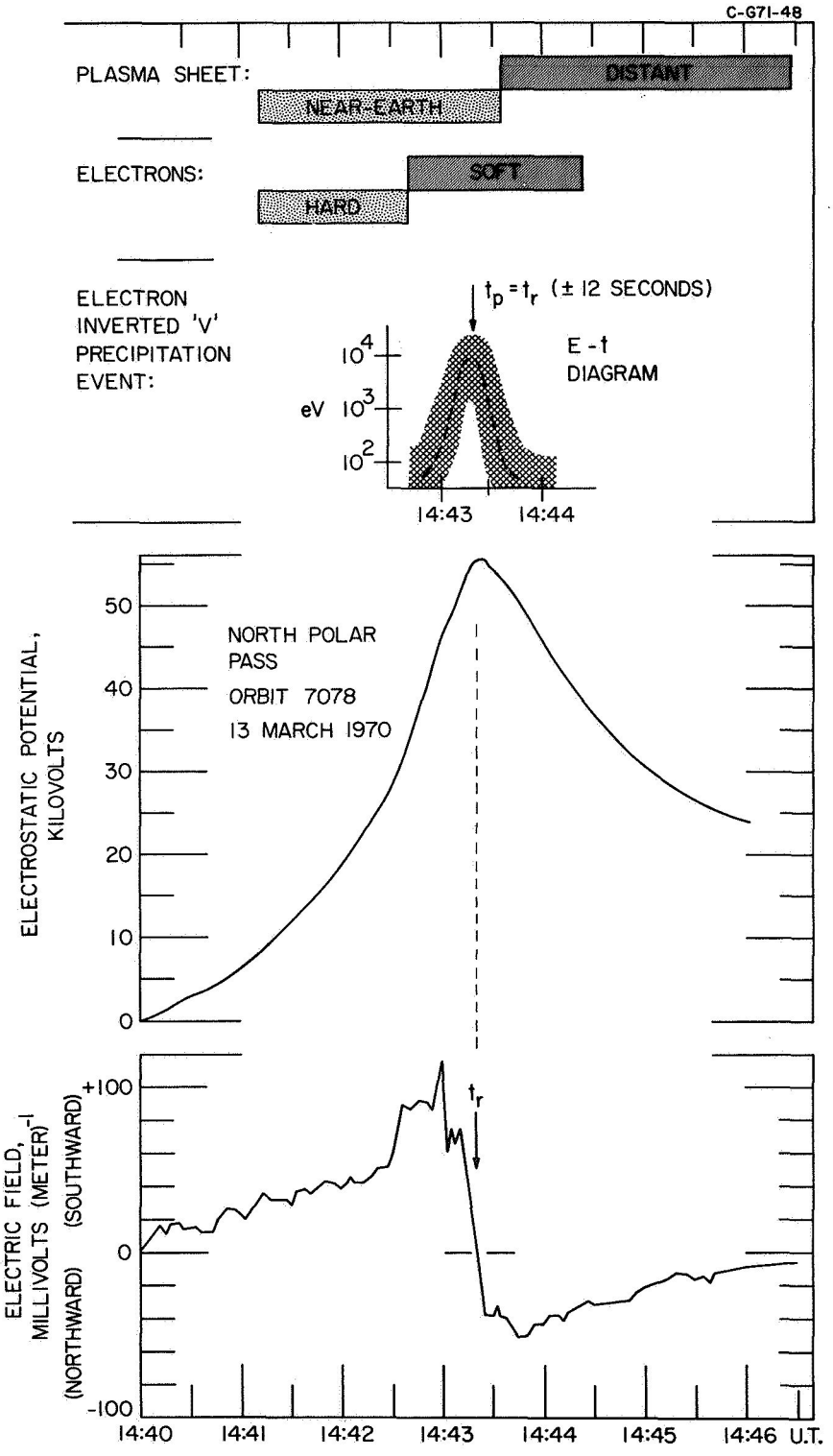
C-G71-48
PLASMA SHEET:
DISTANT
NEAR-EARTH
ELECTRONS:
SOFT
HARD
ELECTRON INVERTED 'V' PRECIPITATION EVENT:
$t_p = t_r$ (± 12 SECONDS)
E - t DIAGRAM
10^4
eV 10^3
10^2
14:43
14:44
NORTH POLAR PASS
ORBIT 7078
13 MARCH 1970
ELECTROSTATIC POTENTIAL, KILOVOLTS
50
40
30
20
10
0
ELECTRIC FIELD, MILLIVOLTS (METER)$^{-1}$
(NORTHWARD) (SOUTHWARD)
+100
0
-100
t_r
14:40
14:41
14:42
14:43
14:44
14:45
14:46 U.T.

Figure 8.

Security Classification

DOCUMENT CONTROL DATA - R&D

(Security classification of title, body of abstract and indexing annotation must be entered when the overall report is classified)

1. ORIGINATING ACTIVITY (Corporate author) University of Iowa Department of Physics and Astronomy	2a. REPORT SECURITY CLASSIFICATION UNCLASSIFIED 2b. GROUP

3. REPORT TITLE

On the Distributions of Plasmas and Electric Fields over the Auroral Zones and Polar Caps

4. DESCRIPTIVE NOTES *(Type of report and inclusive dates)*

5. AUTHOR(S) *(Last name, first name, initial)*

Frank, L. A. and Gurnett, D. A.

6. REPORT DATE	7a. TOTAL NO. OF PAGES	7b. NO. OF REFS
February 24, 1971	49	20

8a. CONTRACT OR GRANT NO.	9a. ORIGINATOR'S REPORT NUMBER(S)
N000-14-68-A-0196-003	U. of Iowa 71-5
b. PROJECT NO.	
c.	9b. OTHER REPORT NO(S) *(Any other numbers that may be assigned this report)*
d.	

10. AVAILABILITY/LIMITATION NOTICES

Distribution of this document is unlimited.

11. SUPPLEMENTARY NOTES	12. SPONSORING MILITARY ACTIVITY
	Office of Naval Research

13. ABSTRACT

SEE PAGES FOLLOWING.

DD FORM 1 JAN 64 1473

Security Classification

14. KEY WORDS	LINK A		LINK B		LINK C	
	ROLE	WT	ROLE	WT	ROLE	WT
Magnetosphere						
Aurora						
Magnetic Storm						
Electric Fields						
Plasma						

INSTRUCTIONS

1. ORIGINATING ACTIVITY: Enter the name and address of the contractor, subcontractor, grantee, Department of Defense activity or other organization *(corporate author)* issuing the report.

2a. REPORT SECURITY CLASSIFICATION: Enter the overall security classification of the report. Indicate whether "Restricted Data" is included. Marking is to be in accordance with appropriate security regulations.

2b. GROUP: Automatic downgrading is specified in DoD Directive 5200.10 and Armed Forces Industrial Manual. Enter the group number. Also, when applicable, show that optional markings have been used for Group 3 and Group 4 as authorized.

3. REPORT TITLE: Enter the complete report title in all capital letters. Titles in all cases should be unclassified. If a meaningful title cannot be selected without classification, show title classification in all capitals in parenthesis immediately following the title.

4. DESCRIPTIVE NOTES: If appropriate, enter the type of report, e.g., interim, progress, summary, annual, or final. Give the inclusive dates when a specific reporting period is covered.

5. AUTHOR(S): Enter the name(s) of author(s) as shown on or in the report. Enter last name, first name, middle initial. If military, show rank and branch of service. The name of the principal author is an absolute minimum requirement.

6. REPORT DATE: Enter the date of the report as day, month, year; or month, year. If more than one date appears on the report, use date of publication.

7a. TOTAL NUMBER OF PAGES: The total page count should follow normal pagination procedures, i.e., enter the number of pages containing information.

7b. NUMBER OF REFERENCES: Enter the total number of references cited in the report.

8a. CONTRACT OR GRANT NUMBER: If appropriate, enter the applicable number of the contract or grant under which the report was written.

8b, 8c, & 8d. PROJECT NUMBER: Enter the appropriate military department identification, such as project number, subproject number, system numbers, task number, etc.

9a. ORIGINATOR'S REPORT NUMBER(S): Enter the official report number by which the document will be identified and controlled by the originating activity. This number must be unique to this report.

9b. OTHER REPORT NUMBER(S): If the report has been assigned any other report numbers *(either by the originator or by the sponsor)*, also enter this number(s).

10. AVAILABILITY/LIMITATION NOTICES: Enter any limitations on further dissemination of the report, other than those imposed by security classification, using standard statements such as:

(1) "Qualified requesters may obtain copies of this report from DDC."

(2) "Foreign announcement and dissemination of this report by DDC is not authorized."

(3) "U. S. Government agencies may obtain copies of this report directly from DDC. Other qualified DDC users shall request through _____."

(4) "U. S. military agencies may obtain copies of this report directly from DDC. Other qualified users shall request through _____."

(5) "All distribution of this report is controlled. Qualified DDC users shall request through _____."

If the report has been furnished to the Office of Technical Services, Department of Commerce, for sale to the public, indicate this fact and enter the price, if known.

11. SUPPLEMENTARY NOTES: Use for additional explanatory notes.

12. SPONSORING MILITARY ACTIVITY: Enter the name of the departmental project office or laboratory sponsoring *(paying for)* the research and development. Include address.

13. ABSTRACT: Enter an abstract giving a brief and factual summary of the document indicative of the report, even though it may also appear elsewhere in the body of the technical report. If additional space is required, a continuation sheet shall be attached.

It is highly desirable that the abstract of classified reports be unclassified. Each paragraph of the abstract shall end with an indication of the military security classification of the information in the paragraph, represented as *(TS), (S), (C), or (U)*.

There is no limitation on the length of the abstract. However, the suggested length is from 150 to 225 words.

14. KEY WORDS: Key words are technically meaningful terms or short phrases that characterize a report and may be used as index entries for cataloging the report. Key words must be selected so that no security classification is required. Identifiers, such as equipment model designation, trade name, military project code name, geographic location, may be used as key words but will be followed by an indication of technical context. The assignment of links, roles, and weights is optional.

DD FORM 1 JAN 64 1473 (BACK)